ROYAL SOCIETY
OF CHEMISTRY

PAPER

Check for updates

Mucus-on-a-chip: investigating the barrier properties of mucus with organic bioelectronics†

Reece McCoy, [ab] Kaixin Wang,[a] Jeremy Treiber,[c] Ying Fu, [d] George G. Malliaras, [b] Alberto Salleo[c] and Róisín M. Owens [*a]

Gastrointestinal (GI) mucus is a biologically complex hydrogel that acts as a partially permeable barrier between the contents of the GI tract and the mucosal epithelial lining. Its structural integrity is essential for the lubrication of the tract thereby aiding smooth transit of contents, and the protection of the epithelium from pathogens that seek to colonise and invade. Understanding its physical response to drugs and the microbiome is essential for treating many gastrointestinal infectious diseases. Given this, a static *in vitro* model of a GI mucus-on-a-chip has been developed with integrated electronics to monitor the barrier properties of mucus hydrogels. Its application for investigating the effect of drugs and biofilm formation on the mucus structure is validated using rheological techniques, confocal microscopy and electrochemical impedance spectroscopy (EIS).

1. Introduction

Gastrointestinal mucus is a dynamic hydrogel that acts as a selective barrier. A healthy, functioning, mucus lining allows the transport of nutrients and biomolecules whilst aiding in preventing invasion from pathogens and foreign material.[1] Impairments to this mucus lining can occur due to the presence of gastrointestinal diseases, as a side effect of medicines and as the result of microbiota dysbiosis. Physical disruption of the mucosal layer not only facilitates the contact of pathogens with epithelial cells, but also allows some normally commensal bacteria to be opportunistic and potentiate disease.[2]

H. pylori, for example, is one of the most common bacterial infections known to cause an impairment of the gastric mucus barrier. It affects approximately 50% of the world's population with about 20% of those experiencing disease phenotypes including peptic ulcers and gastric cancer.[3,4] *H. pylori* is known to secrete urease which hydrolyses urea and elevates the pH of the surrounding environment. With the structural integrity of mucus strongly dependent on pH, a shift from acidic to neutral

conditions causes a sol–gel transition locally and allows bacteria to penetrate further towards the epithelium.[5]

Although mucosal barrier disruption can potentiate disease, it may in limited instances be beneficial, for example, to improve the efficacy of drug treatments of gastrointestinal diseases. *N*-Acetylcysteine (NAC), a potent mucolytic, has been shown to be an effective adjuvant therapy for *H. pylori* eradication,[4,6,7] whilst displaying no activity directly against *H. pylori* itself.[8] The hydrolysis of disulphide bonds by NAC causes a reduction in the viscosity of the mucus, and therefore impairment of the barrier, allowing antibiotics to penetrate further into the bulk and target the pathogen at the epithelial surface. However, it is not a simple case of assuming that therapies known to impair the gastric mucus layer are useful adjuvants to existing antibiotic treatments; for example, in contrast to NAC, Pronase® treatment, in a clinical model as a supplement to the standard triple therapy, was found to have no beneficial effect on the outcome of *H. pylori* treatment, despite its proven efficacy in disrupting the gastric mucus layer.[7,9] *In vitro* models for studying such interactions are therefore useful for testing efficacy of existing medicines or exploring the effects of combination therapies.

The healthy adherent inner mucus layer is generally impermeable to bacteria, which form a dense biofilm in the outer mucus layer (in the case of the colon) or at the interface of the inner mucus layer (in the stomach and small intestine). Biofilms embedded within a mucus layer can limit the efficacy of antibiotics,[10] also shown to not only affect the viability of biofilms but additionally impact on the structure of the outer layer of colonic mucus.[11] Various pathotypes of *E. coli* are known to form biofilms within the intestine with a variety of

a Department of Chemical Engineering and Biotechnology, University of Cambridge, CB3 0AS Cambridge, UK. E-mail: rmo37@cam.ac.uk

b Department of Electrical Engineering, University of Cambridge, CB3 0FA, Cambridge, UK

c Department of Materials Science and Engineering, Stanford University, Stanford, CA, USA

d Department of Pure and Applied Chemistry, University of Strathclyde, G1 1XQ, Glasgow, UK

† Electronic supplementary information (ESI) available. See DOI: **https://doi.org/10.1039/d4tb01351d**

This journal is © The Royal Society of Chemistry 2025

J. Mater. Chem. B, 2025, **13**, 577–587 | 577

mechanisms.[12,13] Pathogenic strains, including enterohaemorrhagic *E. coli* (EHEC), have been show to also disrupt the mucus layer on human colonoids.[14] It is not only pathogenic bacteria that have a direct effect on the structure of mucus. *A. muciniphila*, for example, is known to be beneficial to the integrity of the mucus layer by stimulating the production of additional mucus, producing a thicker, more protective layer. *A. muciniphila* has been shown to degrade and metabolise mucin, produce short chain fatty acids (SCFAs) including butyrate and propionate, which are nutrient sources for goblet cells (the mucus-secreting cells within the intestinal epithelium) and stimulate the production of mucin.[15] Indeed *A. muciniphila* has been found to increase goblet cell distribution in the colon *in vivo*.[16] Understanding the interactions of bacterial species that constitute the microbiome with the mucus layer is important for fully understanding the role they play in potentially potentiating or alleviating disease phenotypes.

As outlined above, there are numerous reasons for which accurate and quantitative models for characterising and assessing the physical integrity of mucus in response to the microbiome, metabolites, and medicines would be useful. Furthermore, to effectively deliver drugs to the epithelial lining, delivery systems must be designed to penetrate the mucus layer without lasting damage or risk of potentiating diease.[17] *In vitro* models can play an important role to screen such systems of benefit to the infectious diseases and drug delivery field,[18] not only for the gastrointestinal tract,[19] but other mucus linings including in the lungs[20] and the vagina too.[21]

The interfacing of biological materials with electronics for quantitative measurements of tissue barrier integrity has developed significantly by the adoption of conducting polymer materials, in particular poly(3,4-ethylenedioxythiophene) doped with polystyrene sulfonate (PEDOT:PSS),[22,23] and we have previously demonstrated the interfacing of PEDOT:PSS electronics with live cells representing the gastrointestinal mucosal layer for monitoring host–microbe interactions.[24] PEDOT:PSS is a blue mixed ionic–electronic conductor with a capacitance that is a function of the volume of the material, in contrast to electrodes made from conventional materials, such as gold, which are not typically transparent and have relatively high impedance. Indium tin oxide (ITO) electrodes, although transparent, also have higher impedance than PEDOT:PSS due to its area-limited capacitance. Semi-optically transparent thin-film PEDOT:PSS microelectrode arrays are compatible with highly sensitive electrical measurements as well as microscopic techniques which permit multimeric and correlative readouts.[25] Common methods of monitoring diffusivity of hydrogels involve the tracking of fluorescent beads with confocal microscopy. Analogously, we can measure the diffusivity of electrochemical probes though such mucus hydrogels but with electrical means rather than optical. Indeed, with the optically transparent nature of PEDOT:PSS devices, conventional optical techniques can also be performed on the same devices enabling correlative measurements.

The focus of this study is to demonstrate a novel method of monitoring the integrity of a gastrointestinal mucus gel and characterising its response to mucolytic compounds and the formation of *E. coli* biofilms on the surface. Including electrochemical sensing can enable the rapid, quantitative, real-time read outs of the state of gastrointestinal mucus and biofilms. This bioelectronic mucus-on-a-chip has a wide range of applications in studying fundamental biochemical mechanisms, drug screening, and biofilm disruption enabling treatment of gastrointestinal bacterial infections.

2. Experimental section

2.1. Synthetic mucus preparation

Mucus hydrogels were prepared as previously described.[26] Purified mucin from porcine stomach type II (PGM, Sigma-Aldrich) was dissolved in physiological buffer (154 mM sodium chloride (Sigma Aldrich), 15 mM monosodium phosphate (Thermo Fisher Scientific, UK), and 3 mM calcium chloride (Thermo Fisher Scientific, UK) at pH 7.4) and stirred for five minutes. The cross-linking reagent 4-arm polyethylene glycol thiol (20 kDa, PEG-4SH, Laysan Bio Inc) was dissolved in physiological buffer before mixing with the PGM solution. Equal volumes of each solution were mixed and stirred at room temperature for three hours until thoroughly mixed. Samples were either stored for 24 h before bulk rheological measurement or immediately transferred into the wells atop corresponding devices for other experiments before gelation. Final concentrations of between 1–5% (m/v) of PGM and PEG-4SH were used.

2.2. Bulk rheological measurement

Rheological properties of the mucus gels were measured with a strain-controlled rheometer (Kinexus Lab +, KNX2112) with a 20 mm parallel plate geometry at 25 °C with a gap of 1 mm. An amplitude sweep dynamic measurement was performed with a strain range from 0.1% to 100% at a frequency of 1 rad s^{-1}. Following the linear viscoelastic region (LVER) determination, a frequency sweep experiment was conducted from 0.1 to 100 rad s^{-1} at 1% strain amplitude to determine the elastic modulus G' (Pa) and viscous modulus G'' (Pa).

2.3. Microstructure analysis

Scanning electron microscopy (SEM) (FEI Nova NanoSEM 450 at 5.00 kV) was used to visualise the porous structure of the mucus gel. Samples were fixed with 2.5% glutaraldehyde (Fisher BioReagents) in phosphate-buffered saline overnight followed by flash freezing in liquid nitrogen, embedding in 2% agarose (Sigma-Aldrich), allowing to set, and then slicing horizontally with a scalpel. The sample was mounted onto carbon tabs on aluminium stubs with the cut side facing up. Finally, samples were coated with 20 nm carbon by sputtering (Combined Coater System, Agar Scientific) before imaging.

2.4. Hydrogel thickness measurement

Glass substrates had a cloning cylinder (8 mm inner diameter, Merck) attached using PDMS (SYLGARD™ 184, Dow) to contain and shape the mucus sample. The well surface was rendered hydrophilic by 30 second plasma treatment with pure oxygen

578 | *J. Mater. Chem. B*, 2025, **13**, 577–587

This journal is © The Royal Society of Chemistry 2025

(Zepto One, Diener electronic). Freshly prepared mucus mimics were pipetted into the well at varying volumes and stored at room temperature for 24 h before confocal laser scanning microscopy (CLSM) imaging. Samples were stained by the addition of 50 $\mu g\ mL^{-1}$ FITC-tagged wheat germ agglutinin in phosphate-buffered saline (WGA-FITC, 2BScientific) for 30 min at room temperature in the dark and rinsed thrice with phosphate-buffered saline. Sample thickness was determined *via* Z-stack (ZEISS LSM 800) at 5× magnification under 488 nm laser illumination. Image analyses were performed *via* ZEN Imaging Software (Version 2.6 blue edition).

2.5. Microelectrode array fabrication

MEAs were fabricated as previously described.[27] Glass wafers (4″) were cleaned in 9:1 sulfuric acid and hydrogen peroxide at 120 °C for 20 minutes. Tracks and contact pads (50 nm Au between two 5 nm Ti adhesion layers) were evaporated (AJA International e-beam evaporator) and patterned using conventional photolithography methods[28] (Heifelberg MLA 150). A SiO_2 insulation layer (230 nm) was deposited by chemical vapor deposition (Plasma-Therm Versaline HDPCVD) and metal tracks and contact pads were photolithographically patterned and exposed with inductively coupled CHF_3 plasma reactive ion etching (Plasma-Therm Versaline ICP etcher). Wafers were treated with O_2 plasma (March Instruments PX-250 Plasma Asher) and a PEDOT:PSS (PH 1000) layer deposited by spin-coating a PH 1000 solution (Heraeus) containing 5% v/v ethylene glycol (EG) and 1% v/v (3-glycidyloxypropyl)trimethyoxysilane (GOPS) at 2000 RPM for 2 min and baked at 140 °C for 30 min. A Ge hard mask (100 nm) was deposited by e-beam evaporation. The Ge and PEDOT:PSS layers were patterned and etched with CF_4 and O_2, respectively. Wafers were diced into individual chips and soaked in deionized water for 48 h to oxidise and remove the Ge layer prior to use.

2.6. Electrochemical characterisation

A PalmSens4 (PalmSens BV, Netherlands) portable potentiostat was used for all electrochemical experiments employing a three-electrode system. The working electrode, counter electrode and reference electrode were the PEDOT:PSS coated gold electrode, a platinum (Pt) mesh and silver/silver chloride (Ag/AgCl) electrode, respectively. The well established electrochemically reversible redox system, 10 mM $K_3Fe(CN)_6/K_4Fe(CN)_6$ + 0.1 M KCl in phosphate-buffered saline was added into the well and the baseline was measured before adding any mucus gel. Freshly prepared mucus, as described previously, was added onto the electrodes and allowed to gel at room temperature overnight before measurement. Cyclic voltammetry (CV) measurements were conducted to locate the peak potentials (E_p) and characterise diffusion coefficient of the ferricyanide probe through the mucus gel. Applied potential range used was −0.5 V to 0.7 V with the scan rate varied between 0.03 V s^{-1} and 0.15 V s^{-1}. EIS measurements were performed using sinusoidal wave with amplitude 0.01 V and frequency range 0.1 Hz to 10^6 Hz coupled to DC potential, using the E_p value (around 0.31 V) from CV scans. PSTrace 5.9 software (PalmSens BV, Netherlands) was used to analyse the data. EIS spectra were fit to the simplified Randles equivalent circuit model using PSTrace 5.9 software. To account for electrode and device variability, which can propagate through all subsequent measurements, all data that is indicated as normalised has been normalised to the baseline data acquired on the same electrode.

2.7. Sample preparation for mucolytic agent treatment

To characterise the mucus barrier after interaction with mucolytics, *N*-acetyl-ʟ-cysteine (NAC, Sigma-Aldrich) at a final concentration of 50 mM, was added (volume of NAC:mucus was 1:1) after gelation (>24 h) and incubated at 37 °C for either 30, 90, or 150 minutes. Rheological and electrochemical measurements were then performed as described above.

2.8. Sample preparation for *E. coli* LF82 interaction

E. coli LF82 was grown overnight, from a glycerol stock, in 5 mL Luria-Bertani broth (LB, formedium) at 37 °C, followed by a 3 h growth in 15 mL fresh LB broth (1% v/v inoculation) at 37 °C, 225 rpm shaking. OD_{600} was measured (BMG Labtech CLARIOstar), culture diluted to 8×10^7 bacteria in 200 μL LB broth and pipetted onto mucus gel (24 hours post-gelation), and allowed to colonise the mucin hydrogels in a static humidified incubator at 37 °C. Following incubation for 2, 6, 12, and 24 hours, the hydrogel samples were gently rinsed with phosphate-buffered saline to remove planktonic and dead bacteria and cell debris. Bacterial distribution was then detected *via* CLSM (488 nm, 10×) by staining bacteria for 1 hour with calcein AM (Invitrogen). EIS measurements were then performed as described above. Spectra were recorded for the baseline and after bacterial incubation for 2, 6, 12 and 24 h. To determine the effect of antibiotics on the biofilm, *E. coli* LF82-colonised mucus samples were treated with 2.5 $\mu g\ mL^{-1}$ trimethoprim in fresh LB broth for 1 h and then imaged with CLSM and again measured with EIS.

2.9. Statistical analysis

Imaging in this study were performed in duplicate and representative images were selected to show the results. All data are shown in form of mean ± standard deviation (SD) calculated for at least three repetitions ($n \geq 3$) unless otherwise indicated in figure caption. Graphing and statistical analysis was performed in GraphPad Prism 9 (GraphPad Software, USA) and Origin Pro (OriginLab Corporation, MA, USA). A one-way analysis of variance (ANOVA) with Tukey's *post hoc* correction (95% C.I.) was performed to compare the significant differences between multiple groups. A two-way ANOVA was performed to compare data in multiple groups with two independent variables. Statistically significant is denoted as: ns = not significant, $p < 0.05$ (*), $p < 0.01$ (**), $p < 0.001$ (***) and $p < 0.001$ (****).

3. Results and discussion

3.1. Rheological characterisation of mucus gel

The strategy employed here to produce *in vitro* mucus mimics was originally proposed by Joyner *et al.*[29] By tuning the ratio of porcine gastric mucus (PGM) and a PEGylated-4arm-thiol

This journal is © The Royal Society of Chemistry 2025

J. Mater. Chem. B, 2025, **13**, 577–587 | **579**

crosslinker, the viscoelastic properties of the mucus hydrogel was tuneable within the range of *in vivo* mucus (Fig. 1(A)). The properties of the prepared mucus hydrogels were previously investigated with particle tracking microrheology and demonstrated to have physiological relevance. This work inspired us to consider how the properties of mucus hydrogels could be

monitored both optically and electrically for a quantitative readout of barrier properties. We first aimed to replicate a viscoelastic hydrogel that mimics the rheological properties of native gastrointestinal mucus. Fixed-frequency amplitude sweep experiments were performed from 0.1–10% strain with a frequency of 1 rad s^{-1} and elastic behaviour observed where
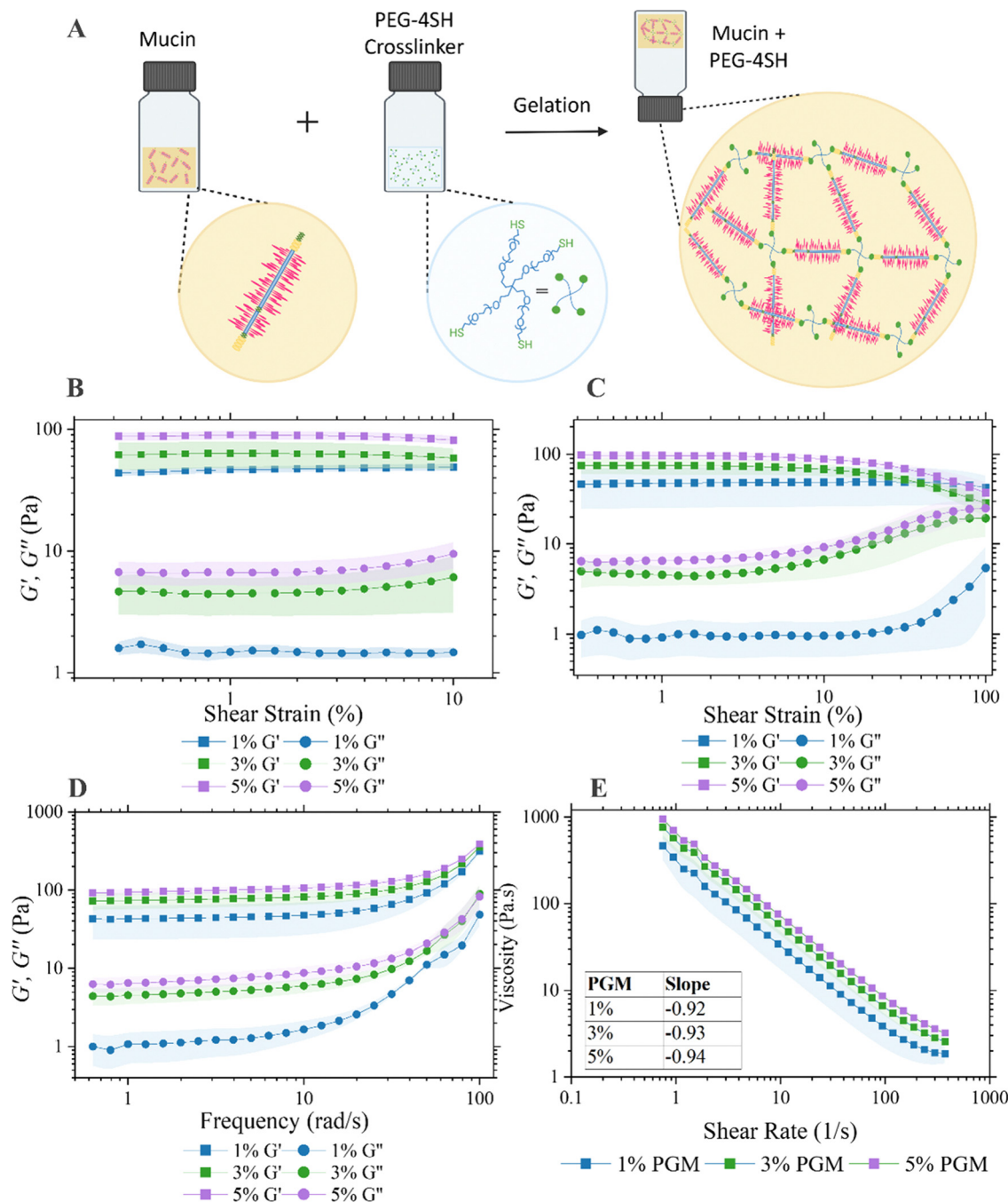
Fig. 1 (A) Schematic of mucus formation steps demonstrating the action of the PEG-4SH crosslinker in joining mucin molecules together. (B) Bulk rheological measurements of synthetic mucus were generated by mixing 2% PEG-4SH with 1%, 3%, and 5% PGM (resulting concentration) respectively. G' represents elastic modulus (squares) and G'' represents viscous modulus (circles). Linear viscoelastic region (LVER) of the hydrogel is obtained *via* amplitude sweep dynamic measurement (0.1% to 10% shear strain, frequency = 1 rad s^{-1}); (C) amplitude sweep with a larger range containing the upper limit of the LVER – the critical strain. (D) Frequency sweep at strain = 1% from 0.1 to 100 rad s^{-1}; (E) viscosity curve for synthetic mucus ($n \geq 3$, *$p < 0.05$, **$p < 0.01$).

G' exceeded G'' at low shear strains confirming the formation of the gel structure (Fig. 1(B) and (D)). A review of the literature reports G' values between ~ 3–100 Pa from *ex vivo* and *in vitro* models and demonstrate that this increases along the GI tract.[30] Another study which measured the G' from the stomach to the distal colon of a porcine model showed a general increase from ~ 10–200 Pa with progression along the GI tract.[31] G' values at 1 rad s^{-1} for the mucus mimics in this study are approximately 50 Pa, 70 Pa and 100 Pa as the PGM concentration is increased from 1% to 3% to 5%. This sits firmly within the range of literature reported values and demonstrates the tunability of the model to the rheological properties of mucus spanning regions of the GI tract. At 1% PGM, the mucus gels displayed higher viscoelasticity than the 3% and 5% samples as demonstrated by the greater degree of separation between the G' and G'' profiles. The critical shear strain varied by PGM concentration which was found to be 40% for 1% PGM and 15% for both 3% and 5% PGM samples (Fig. 1(C)). Graphs of the loss factor varying with both frequency and strain independently are below the flow point at $\tan(\delta) = 1$ across the entire region investigated (ESI†, Fig. S1). This demonstrates dominant elasticity which is shown to approach the crossover point of G'' to G' at strains approach 100%.

Mucus viscosity was determined by sweeping the applied shear rate. All samples displayed shear thinning behaviour and indeed the slope of the flow curve for all samples, as shown on (Fig. 1(E)), was approximately -1 as demonstrated previously.[32] The range of physiological shear rates *in vivo* has been reported as 1–10 s^{-1}.[33] G' and G'' of the semi-synthetic mucus described is within the range of that of other *ex vivo* and biosimilar mucus models found in the literature at a shear rate of 1 s^{-1}. One particular study by Barmpatsalou *et al.* demonstrated the viscosity of porcine intestinal mucus varying across the intestine with small intestine regions (duodenum ~ 80 Pa s, jejunum ~ 30 Pa s and ileum ~ 150 Pa s) exhibiting lower viscosity than colonic mucus (proximal colon ~ 180 Pa s, distal colon ~ 300 Pa s) except for the cecum which had significantly lower viscosity than all other regions (< 10 Pa s).[31] The corresponding apparent viscosities of the mucus investigated within this study range from between ~ 300–700 Pa s as the PGM concentration increases. Disease states, including cystic fibrosis, can exhibit almost 2-fold higher viscosities of mucin glycoproteins relative to healthy controls,[34] emphasising the tunability of the mucus model used in this study for modelling various pathological conditions. Attempts were also made to extract mucus from the goblet cell-like cell line HT29-MTX which has been shown to secrete mucin. Extracted mucus failed to predictably form homogenous gels and thus validated our reasoning for continuing with the semi-synthetic approach (ESI,† Fig. S2).

The swelling ratio, a fractional measure of water absorption by the material, was determined for each concentration of PGM used in this study and ranged from ~ 9–13 (ESI,† Fig. S3). The values are similar to that determined in the literature to a similar mucus mimic, albeit with a different ratio of cross-linking agent to PGM.[35] Furthermore, mucus in the large intestine is reported to have a water content of 93–95%, and

thus a dry mass of 5–7% of the total weight.[36,37] The dry mass would swell between 13–19 times to reach the reported literature water content values, with the semi-synthetic mucus model described here being at the lower end of this range.

Whilst the exclusive use of commercially available porcine gastric mucin lacks the ability to form a stable mucus gel that mimics natural mucus,[38] the rational approach proposed by Joyner *et al.* allows for the formation of stable mucus gels that mirror the natural thiol-mediated structures and rheology and enables usage in applications where large quantities are required.

3.2. Electrochemical characterisation of mucus gel

To electrically assess the barrier properties of the mucus gel, cyclic voltammetry (CV) and electrochemical impedance spectroscopy (EIS) were used. The electrochemical set up (Fig. 2(A)–(C)) includes a microelectrode array with 500 μm PEDOT:PSS square working electrodes, silver–silver chloride reference electrode and a large platinum mesh counter electrode. A well bonded to the glass substrate contained the electrolyte of the three electrode electrochemical cell. PEDOT:PSS was coated on top of gold electrodes with some electrodes being solid gold, and others comprised of only an outline of gold thus creating an optically transparent surface that is usful for correlating electrical readouts with optical microscopy.[31]

To interface the device with mucus, substrates were O$_2$ plasma treated to improve wetability and surface contact for the mucus which was added to the well and allowed to gel. Upon gelation, the porous structure of the mucus was formed as shown by SEM, although this method of imaging cannot truly represent the structure of the mucus mimic due to the numerous processing steps necessary to fix, dessicate, slice, and sputter coat the sample before imaging (Fig. 2(D)). Due to the wetability of the glass surface and the attached well, the mucus hydrogel wetted the walls and formed a slight concave meniscus and as such Z-stacks were taken with confocal microscopy (Fig. 2(E)) to measure the actual thickness of mucus and determine the centre vs edge variance (ESI,† Fig. S4). The mucus was thicker at the edges and as such a radial electrode array design would be beneficial for minimising this variance in future studies.

CV was first conducted to determine the electrochemical response of the typical potassium ferricyanide/ferrocyanide redox couple (Fig. 2(F)). The anodic peak potential in this system was determined to be +0.31 V which was used as the E_{DC} potential in later EIS measurements. The thickness of the mucus layer was intially varied with both CV and EIS being performed to determine the response to increasing mucus thickness on the charge transfer resistance. CV scans, performed at a range of scan rates, demonstrate diminishing oxidation and reduction current peaks in response to thicker mucus gels and indeed, extracted diffusion values and computed electron transfer rates (ESI,† Fig. S5) demonstrate the increased resistance to the redox probe at greater thicknesses. The non-linear trend can likely be attributed to the tortuosity of the intricate porous structure of mucus. Indeed, as the mucus volume, and thus thickness, was increased, an increase in extracted resistance values was observed (Fig. 2(H)). A representitive Nyquist plot for this system is shown with increasing mucus thickness (Fig. 2(G)). This confirms the three electrode electrochemical system
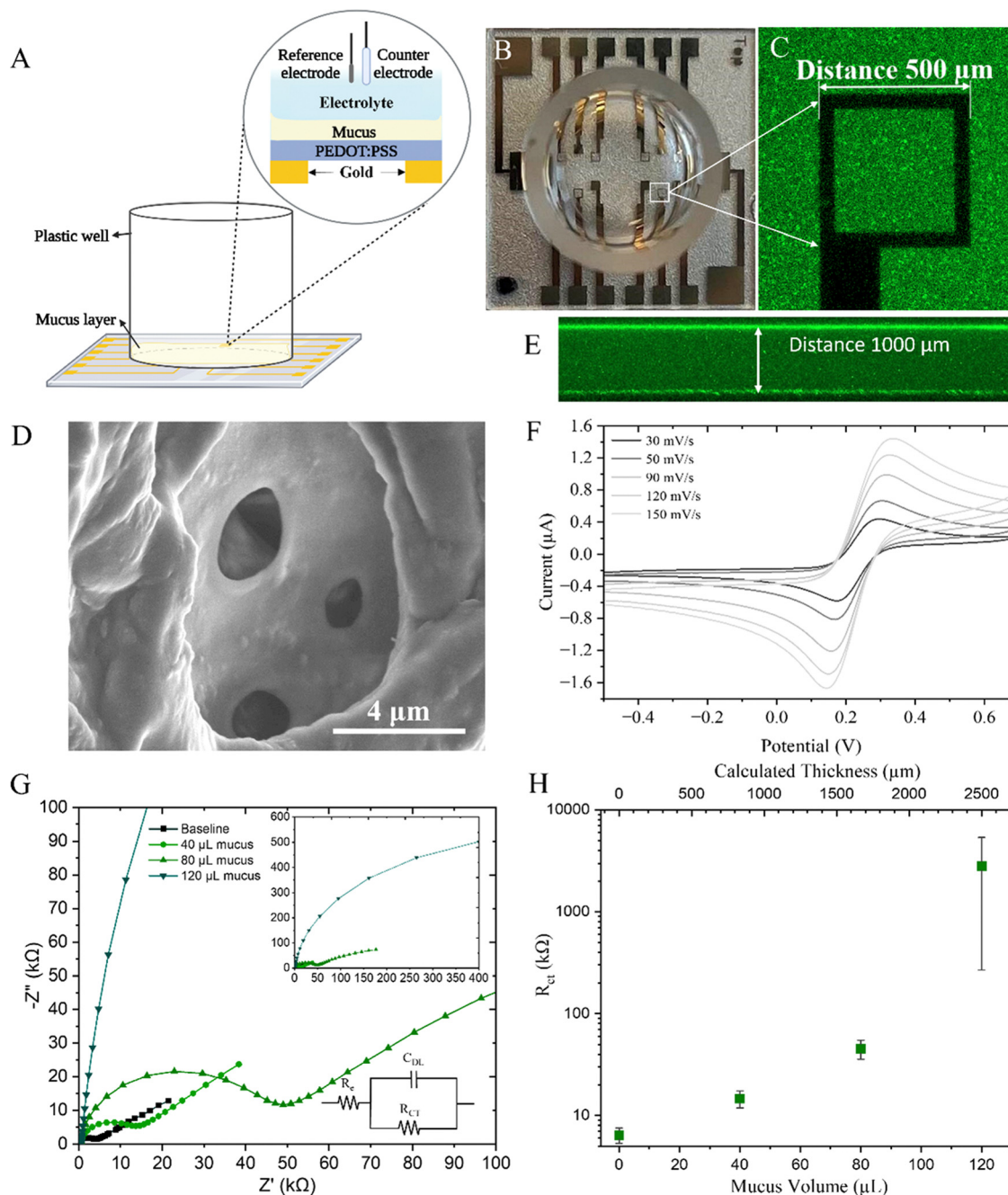
This journal is © The Royal Society of Chemistry 2025

J. Mater. Chem. B, 2025, **13**, 577–587 | 581

Fig. 2 (A) Schematic illustration of mucus on MEAs assembling with twelve PEDOT:PSS-coated gold working electrodes (https://Biorender.com). (B) Top view of the chip, and (C) confocal image of a square working electrode (showing 500 μm width). Mucus is stained with WGA-FITC lectin as shown in green. (D) SEM image of 5% PGM hydrogel used in electrical experiments. Scale bar 4 μm. (E) Example Z-stack of the mucus layer stained with WGA-FITC allowing for determination of mucus thickness on individual transparent electrodes. (F) Cyclic voltammetry (scan rates 30, 50, 90, 120, and 150 mV s^{-1}) of 10 mM $[Fe(CN)_6]^{3-/4-}$ with 0.1 M KCl, in phosphate-buffered saline on 1000 μm mucus (5% PGM + 2% PEG-4SH) coated on the electrode surface. Potential is *vs.* Ag/AgCl. (G) Representative Nyquist plot at varying mucus thickness with simplified Randles circuit inset and a zoomed out of the same data inset to capture the full data range, and (H) extracted charge transfer resistance with varying mucus volume within the well atop the MEA. Error bar denotes standard deviation with n = 5 electrodes.

can be used for a quantitative readout of charge transfer resistance as a result of mucus presence atop the PEDOT:PSS electrode which increases with increased mucus thickness.

3.3. Mucolytic effect on mucin gel

N-Acetylcysteine (NAC) is a well-known mucolytic agent that has found clinical uses, particularly for acute and chronic lung conditions[39] and, additionally, its ability to disrupt bacterial biofilms has been demonstrated *in vitro* and in clinical studies.[40] NAC decreases mucus viscosity (Fig. 3(A)) by causing a substitution of disulfide bonds between cysteine residues in the mucin network with free sulfhydryl groups.[41]

The impact of NAC treatment on the microstructure of mucus was demonstrated with electrochemical techniques.

582 | *J. Mater. Chem. B*, 2025, **13**, 577–587

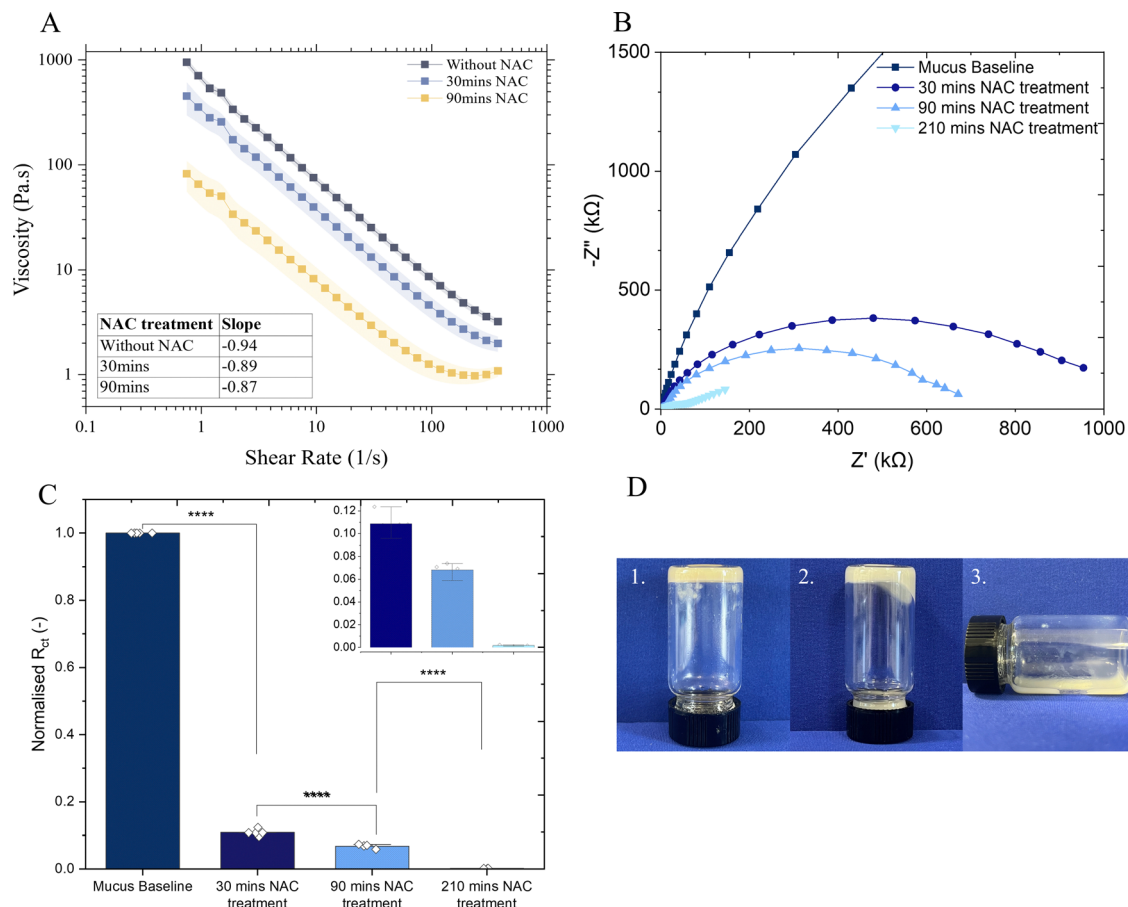This journal is © The Royal Society of Chemistry 2025

Fig. 3 Effect of NAC on mucus properties. (A) Apparent viscosity of mucus without NAC treatment (black), after 30 min (blue) and 90 min (yellow) as extracted from frequency sweep measurement. (B) Representative Nyquist plot of NAC treatment EIS data. (C) Graph of normalised charge transfer resistance (R_{ct}) with increasing NAC treatment times, and (D) Images of mucus samples begore and after NAC treatment. From left to right: 1. synthetic mucus (gelation); 2. 90 min NAC treatment; 3. 24 h NAC treatment. (Error bars denote standard deviation. $n \geq 4$, $n = 2$ for 210 min NAC treatment *$p < 0.05$, **$p < 0.01$, ****$p < 0.0001$.)

EIS measurements demonstrate the decrease in charge transfer resistance (R_{ct}) to ferrocyanide probe upon incubation with NAC (Fig. 3(B)) and the R_{ct} of the mucus after 30 minutes incubation declined markedly to only one tenth the value observed in mucus prior to NAC treatment (Fig. 3(C)), validating these techniques in measuring the breakdown of the hydrogel matrix. CV measurements exhibited a sevenfold increase in the diffusivity of the redox probe ($p < 0.05$) following 150 min of NAC treatment (ESI,† Fig. S6). Furthermore, incubation of a bulk mucus gel with 50 mM NAC visibly showed breakdown of the gel matrix (Fig. 3(D)) whereby the gel visibly deformed and began to flow after 90 minutes, and appeared liquid after 24 hours. Corresponding rheology data is provided in ESI,† Fig. S7.

3.4. Characterisation of *E. coli* LF82 biofilm formation and disruption

The healthy adherent mucus layer found in the stomach and the small intestine are normally impenetrable to commensal bacteria. The outer mucus layer found in the colon is known to host the microbiome within its bulk. This study aimed to form

a biofilm at the interface of the adherent mucus layer as would be the case *in vivo*. The adherent-invasive *E.coli* (AIEC) strain LF82 is of particular interest to those researching irritable bowel disease (IBD) due to its implication in Crohn's disease,[42] and indeed, the treatment of a murine colitis model with *E. coli* LF82 has been shown to exacerbate fibrosis.[43] With its ability to form biofilm structures, particularly intracellularly, LF82 has defensive mechanisms which are known to enhance resistance to antibiotics and the host immune system.[44] The addition of *E. coli* LF82 to the mucus-on-a-chip model was found to show features of attachment, growth, colonisation and dispersion atop the mucus gel over a 24 h period (Fig. 4(A)). Similar trends are observed for a green fluorescence protein (GFP)-expressing *E. coli* BL21 (ESI,† Fig. S8), where depth profile images show clear maturation of the biofilm with successive incubation timepoints and significant biofilm height after a 24 h period. Such observations are further supported by a microtiter crystal violet assay[45,46] to determine bulk biofilm biomass demonstrating increase in at all time points relative to a blank mucus sample, and a significant increase post 24 h incubation (ESI,† Fig. S9). This technique is useful for

This journal is © The Royal Society of Chemistry 2025
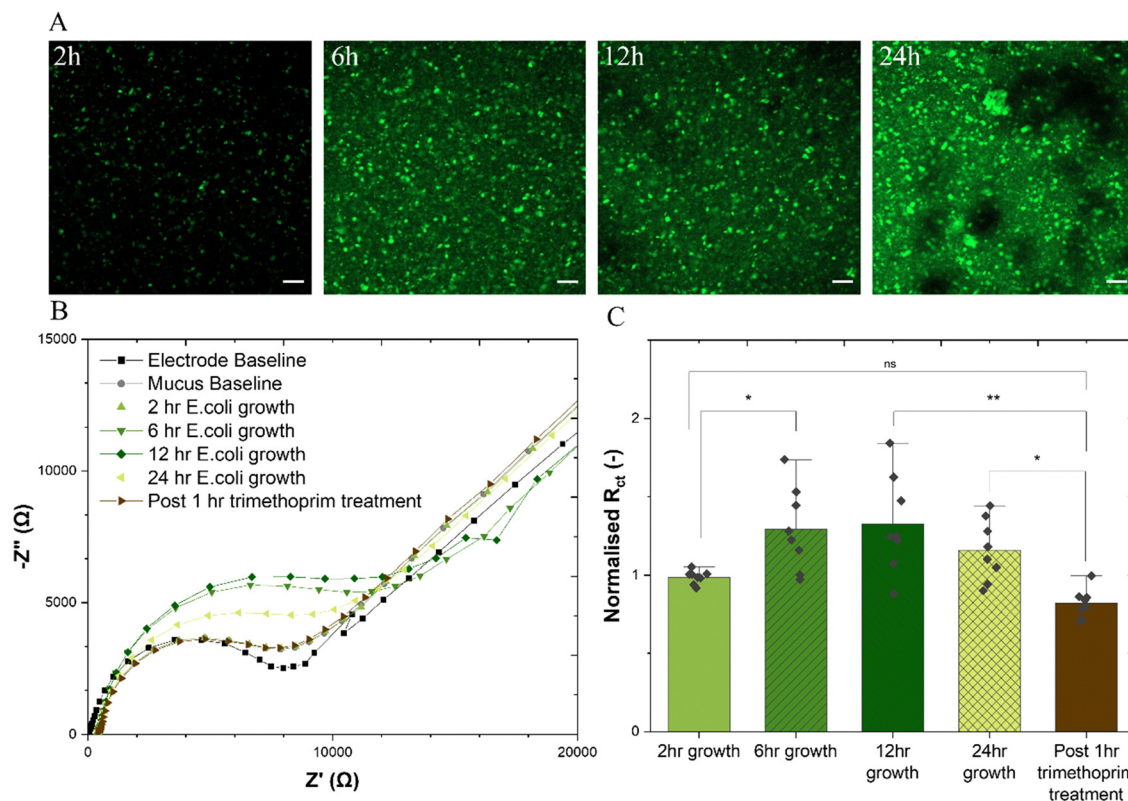
J. Mater. Chem. B, 2025, **13**, 577–587 | **583**

Fig. 4 (A) Representative confocal images of *E. coli* LF82 in different stages of biofilm formation on top of mucus layer (5% PGM with 2% PEG-4SH). Confocal images from left to right: 2 h, 6 h, 12 h and 24 h incubation periods of *E.coli* LF82 atop mucus gel stained with Calcein AM. Scale bar = 50 μm. (B) Representative Nyquist plots of device baseline, addition of mucus layer before *E. coli* LF82, after incubation (2, 6, 12 and 24 h) and post 1 hour antibiotic treatment. (C) Summarised mucus relative charge transfer resistances (normalised to the mucus-only baseline on the same electrode) from EIS characterisation. Error bars denote standard deviation (ns = not significant, *$p < 0.05$, **$p < 0.01$).

quantifying whole biofilm due to its ability to stain negatively charged biologically molecules including polysaccharide and extracellular DNA which are important constituents of the biofilm.[47] (Fig. 4(B)) shows a representative Nyquist plot for each experimental group including electrode and mucus baseline, measurements at each bacterial growth time point, and post antibiotic treatment. All extracted resistance datapoints ((Fig. 4(C)) are normalised to the charge transfer resistance of the mucus-only baselines. Increase in the charge transfer resistance is measured after 6 h of bacterial growth which peaks at a relative increase of 33% after 12 h growth, stabilises, and diminishes by the 24 h timepoint. There is thus no statistical difference between the 24 h charge transfer resistance and that of the 2 h group, likely because of loss of biofilm due to the shedding dispersion phase of biofilm growth whereby significant proportions of the biofilm are detached.[48,49] Following this period, the addition of 2.5 μg mL^{-1} trimethoprim, demonstrated to have strong inhibitory activity against the *E. coli* LF82 strain (ESI,† Fig. S10) was found to exhibit a statistically significant decrease in the charge transfer resistance. This technique is able to monitor the growth of *E. coli* LF82 biofilms on a mucus layer and the effect of antibiotics on the biofilm with integrated sensing for quantitative readouts. Indeed, such a technique could be useful for quantitatively monitoring biofilm formation with different bacterial growth conditions which include varying

growth factors and media compositions but also, for example, exposure to western diets rich in specific polysaccharides that promote biofilm formation and dysbiosis.[50] It had been previously demonstrated that, compared with well known biofilm-forming organism *P. aeruginosa*, *E. coli* LF82 biofilms are significantly impacted not only by antibiotic dosage, but also fluid flow and thus shear stress.[51] The bioelectronic mucus model presented here could be adapted to introduce fluid flow with integrated electronics to provide real time monitoring of biofilm prevention, formation, and treatment with rapid, quantitative readouts within the context of the gastrointestinal tract, or other mucosal surfaces. Furthermore, the incubation of mucolytic, non-biofilm forming bacteria with the model under different treatments could be useful for determining growth rates when cultured on the mucus gels due to the ability to track mucus disruption, or determine a particular strain's ability to degrade mucin. It is crucial to understand how bacterial species within the microbiome interact with the mucus layer to fully comprehend their role in either exacerbating or alleviating disease symptoms.

4. Conclusions

The gastrointestinal mucosal layer is a biologically complex hydrogel which serves as a vital, partially permeable, barrier

contributing to structural integrity, lubrication, and protection of the GI tract against pathogens. Monitoring the mucosal layer is important for understanding host–microbiome interactions and effect of drugs on the layer and integrated sensing capabilities allow for real time monitoring of such interactions. This study presents an *in vitro* model of a gastrointestinal (GI) mucus integrated on a microelectrode array, providing a useful tool for understanding the resistive properties of the mucus when exposed to drugs or bacteria. The model was validated through confocal microscopy, cyclic voltammetry and EIS, enabling the exploration of the impact of mucolytic drugs and *E. coli* biofilm formation on bulk electrical properties and therefore bulk mucus structure. Such a tool is valuable for advancing our understanding of gastrointestinal infectious diseases affecting the mucosal lining and refining treatment strategies.

Author contributions

RM conceived the study. RM and KW performed experiments and analysed the data. RM wrote the manuscript. JT and AS oversaw, designed, and produced the microelectrode arrays used for experiments. RMO and GGM supervised RM and RMO secured financial support. RMO and YF edited the final manuscript. All authors approved the final manuscript.

Data availability

Data for this article, including electrochemical impedance spectroscopy, rheology and confocal imaging, are available at Apollo, University of Cambridge, at 10.17863/CAM.109555.

Conflicts of interest

The authors declare no conflicts of interest.

Acknowledgements

References

1 M. E. V. Johansson, H. Sjövall and G. C. Hansson, The Gastrointestinal Mucus System in Health and Disease, *Nat. Rev. Gastroenterol. Hepatol.*, 2013, **10**(6), 352–361, DOI: **10.1038/nrgastro.2013.35**.

2 Q. Zhao and C. L. Maynard, Mucus, Commensals, and the Immune System, *Gut Microbes*, 2022, **14**(1), DOI: **10.1080/19490976.2022.2041342**.

3 Y. Li, H. Choi, K. Leung, F. Jiang, D. Y. Graham and W. K. Leung, Global Prevalence of Helicobacter Pylori Infection between 1980 and 2022: A Systematic Review and Meta-Analysis, *Lancet Gastroenterol. Hepatol.*, 2023, **8**(6), 553–564, DOI: **10.1016/S2468-1253(23)00070-5**.

4 L. E. S. Fontes, A. L. C. Martimbianco, C. Zanin and R. Riera, *N*-Acetylcysteine as an Adjuvant Therapy for Helicobacter Pylori Eradication, *Cochrane Database Syst. Rev.*, 2019, (2), DOI: **10.1002/14651858.CD012357.pub2**.

5 J. P. Celli, B. S. Turner, N. H. Afdhal, S. Keates, I. Ghiran, C. P. Kelly, R. H. Ewoldt, G. H. McKinley, P. So, S. Erramilli and R. Bansil, Helicobacter Pylori Moves through Mucus by Reducing Mucin Viscoelasticity, *Proc. Natl. Acad. Sci. U. S. A.*, 2009, **106**(34), 14321–14326, DOI: **10.1073/pnas.0903438106**.

6 C. D. Tran, S. Kritas, M. A. F. Campbell, H. Q. Huynh, S. S. Lee and R. N. Butler, Novel Combination Therapy for the Eradication of Helicobacter Pylori Infection in a Mouse Model, *Scand. J. Gastroenterol.*, 2010, **45**(12), 1424–1430, DOI: **10.3109/00365521.2010.506245**.

7 H. Yoon and D. H. Lee, Mucolytics as Adjuvant Agent to Improve Helicobacter Pylori Eradication Rate: Still Long and Winding Road to Positive Results, *Gut and Liver*, ed. J. B. Chung, 2015, pp. 257–258, DOI: **10.5009/gnl15117**.

8 A. K. Gurbuz, A. M. Ozel, R. Ozturk, S. Yildirim, Y. Yazgan and L. Demirturk, Effect of N-Acetyl Cysteine on Helicobacter Pylori, *South. Med. J.*, 2005, **98**(11), 1095–1097, DOI: **10.1097/01.smj.0000182486.39913.da**.

9 C. S. Bang, Y. S. Kim, S. H. Park, J. B. Kim, G. H. Baik, K. T. Suk, J. H. Yoon and D. J. Kim, Additive Effect of Pronase on the Eradication Rate of First-Line Therapy for Helicobacter Pylori Infection, *Gut Liver*, 2015, **9**(3), 340–345, DOI: **10.5009/gnl13399**.

10 S. Frisch, A. Boese, B. Huck, J. C. Horstmann, D.-K. Ho, K. Schwarzkopf, X. Murgia, B. Loretz, C. de Souza Carvalho-Wodarz and C.-M. Lehr, A Pulmonary Mucus Surrogate for Investigating Antibiotic Permeation and Activity against Pseudomonas Aeruginosa Biofilms, *J. Antimicrob. Chemother.*, 2021, **76**(6), 1472–1479, DOI: **10.1093/jac/dkab068**.

11 C.-Y. Chen, K.-C. Hsu, H.-Y. Yeh and H.-C. Ho, Visualizing the Effects of Antibiotics on the Mouse Colonic Mucus Layer, *Tzu Chi Med. J.*, 2020, **32**(2), 145, DOI: **10.4103/tcmj.tcmj_70_19**.

This journal is © The Royal Society of Chemistry 2025

J. Mater. Chem. B, 2025, **13**, 577–587 | 585

12 D. K. Govindarajan, N. Viswalingam, Y. Meganathan and K. Kandaswamy, Adherence Patterns of Escherichia Coli in the Intestine and Its Role in Pathogenesis, *Med. Microecol.*, 2020, **5**, 100025, DOI: **10.1016/j.medmic.2020.100025**.

13 E. Rossi, A. Cimdins, P. Lüthje, A. Brauner, Å. Sjöling, P. Landini and U. Römling, "It's a Gut Feeling"–Escherichia Coli Biofilm Formation in the Gastrointestinal Tract Environment, *Critical Reviews in Microbiology*, Taylor and Francis Ltd, 2018, pp. 1–30, DOI: **10.1080/1040841X.2017.1303660**.

14 J. In, J. Foulke-Abel, N. C. Zachos, A.-M. Hansen, J. B. Kaper, H. D. Bernstein, M. Halushka, S. Blutt, M. K. Estes, M. Donowitz and O. Kovbasnjuk, Enterohemorrhagic Escherichia Coli Reduces Mucus and Intermicrovillar Bridges in Human Stem Cell-Derived Colonoids, *Cell. Mol. Gastroenterol. Hepatol.*, 2016, **2**(1), 48–62, DOI: **10.1016/j.jcmgh.2015.10.001**.

15 N. Burger-van Paassen, A. Vincent, P. J. Puiman, M. van der Sluis, J. Bouma, G. Boehm, J. B. van Goudoever, I. van Seuningen and I. B. Renes, The Regulation of Intestinal Mucin MUC2 Expression by Short-Chain Fatty Acids: Implications for Epithelial Protection, *Biochem. J.*, 2009, **420**(2), 211–219, DOI: **10.1042/BJ20082222**.

16 L. Zhu, X. Lu, L. Liu, J. Voglmeir, X. Zhong and Q. Yu, Akkermansia Muciniphila Protects Intestinal Mucosa from Damage Caused by *S. Pullorum* by Initiating Proliferation of Intestinal Epithelium, *Vet. Res.*, 2020, **51**(1), 34, DOI: **10.1186/s13567-020-00755-3**.

17 L. M. Ensign, R. Cone and J. Hanes, Oral Drug Delivery with Polymeric Nanoparticles: The Gastrointestinal Mucus Barriers, *Adv. Drug Delivery Rev.*, 2012, **64**(6), 557–570, DOI: **10.1016/j.addr.2011.12.009**.

18 T. L. Carlson, J. Y. Lock and R. L. Carrier, Engineering the Mucus Barrier, *Annu. Rev. Biomed. Eng.*, 2018, **20**(1), 197–220, DOI: **10.1146/annurev-bioeng-062117-121156**.

19 R. McCoy, S. Oldroyd, W. Yang, K. Wang, D. Hoven, D. Bulmer, M. Zilbauer and R. M. Owens, *In Vitro* Models for Investigating Intestinal Host–Pathogen Interactions, *Adv. Sci.*, 2024, **11**(8), DOI: **10.1002/advs.202306727**.

20 G. A. Duncan, J. Jung, J. Hanes and J. S. Suk, The Mucus Barrier to Inhaled Gene Therapy, *Mol. Ther.*, 2016, **24**(12), 2043–2053, DOI: **10.1038/mt.2016.182**.

21 G. Lacroix, V. Gouyer, F. Gottrand and J.-L. Desseyn, The Cervicovaginal Mucus Barrier, *Int. J. Mol. Sci.*, 2020, **21**(21), 8266, DOI: **10.3390/ijms21218266**.

22 R. M. Owens and G. G. Malliaras, Organic Electronics at the Interface with Biology, *MRS Bull.*, 2010, **35**(6), 449–456, DOI: **10.1557/mrs2010.583**.

23 M. J. Donahue, A. Sanchez-Sanchez, S. Inal, J. Qu, R. M. Owens, D. Mecerreyes, G. G. Malliaras and D. C. Martin, Tailoring PEDOT Properties for Applications in Bioelectronics, *Mater. Sci. Eng., R*, 2020, **140**, 100546, DOI: **10.1016/j.mser.2020.100546**.

24 C. M. Moysidou, D. C. van Niekerk, V. Stoeger, C. Pitsalidis, L. A. Draper, A. M. Withers, K. Hughes, R. McCoy, R. Acharya, C. Hill and R. M. Owens, Modelling Human Gut-Microbiome Interactions in a 3D Bioelectronic Platform, *Small Sci.*, 2024, **4**(6), DOI: **10.1002/smsc.202300349**.

25 S. Middya, V. F. Curto, A. Fernández-Villegas, M. Robbins, J. Gurke, E. J. M. Moonen, G. S. Kaminski Schierle and G. G. Malliaras, Microelectrode Arrays for Simultaneous Electrophysiology and Advanced Optical Microscopy, *Adv. Sci.*, 2021, **8**(13), DOI: **10.1002/advs.202004434**.

26 K. Joyner, D. Song, R. F. Hawkins, R. D. Silcott and G. A. Duncan, A Rational Approach to Form Disulfide Linked Mucin Hydrogels, *Soft Matter*, 2019, **15**(47), 9632–9639, DOI: **10.1039/c9sm01715a**.

27 K. Bali, R. McCoy, Z. Lu, J. Treiber, A. Savva, C. F. Kaminski, G. Salmond, A. Salleo, I. Mela, R. Monson and R. M. Owens, Multiparametric Sensing of Outer Membrane Vesicle-Derived Supported Lipid Bilayers Demonstrates the Specificity of Bacteriophage Interactions, *ACS Biomater. Sci. Eng.*, 2023, **9**(6), 3632–3642, DOI: **10.1021/acsbiomaterials.3c00021**.

28 Q. Thiburce, N. Melosh and A. Salleo, Wafer-Scale Microfabrication of Flexible Organic Electrochemical Transistors, *Flexible Printed Electron.*, 2022, **7**(3), 034001, DOI: **10.1088/2058-8585/ac808a**.

29 K. Joyner, D. Song, R. F. Hawkins, R. D. Silcott and G. A. Duncan, A Rational Approach to Form Disulfide Linked Mucin Hydrogels, *Soft Matter*, 2019, **15**(47), 9632–9639, DOI: **10.1039/C9SM01715A**.

30 L. Sardelli, D. P. Pacheco, A. Ziccarelli, M. Tunesi, O. Caspani, A. Fusari, F. B. Vangosa and P. Petrini, Towards Bioinspired *in Vitro* Models of Intestinal Mucus, *RSC Adv.*, 2019, 15887–15899, DOI: **10.1039/c9ra02368b**.

31 V. Barmpatsalou, I. R. Dubbelboer, A. Rodler, M. Jacobson, E. Karlsson, B. L. Pedersen and C. A. S. Bergström, Physiological Properties, Composition and Structural Profiling of Porcine Gastrointestinal Mucus, *Eur. J. Pharm. Biopharm.*, 2021, **169**, 156–167, DOI: **10.1016/j.ejpb.2021.10.008**.

32 J. P. Celli, B. S. Turner, N. H. Afdhal, R. H. Ewoldt, G. H. McKinley, R. Bansil and S. Erramilli, Rheology of Gastric Mucin Exhibits a PH-Dependent Sol−Gel Transition, *Biomacromolecules*, 2007, **8**(5), 1580–1586, DOI: **10.1021/bm0609691**.

33 A. K. Hardacre, R. G. Lentle, S.-Y. Yap and J. A. Monro, Predicting the Viscosity of Digesta from the Physical Characteristics of Particle Suspensions Using Existing Rheological Models, *J. R. Soc., Interface*, 2018, **15**(142), 20180092, DOI: **10.1098/rsif.2018.0092**.

34 B. L. Siomiany, V. L. N. Murty, S. R. Carter and A. Slomiany, Effect of Covalently Bound Fatty Acids and Associated Lipids on the Viscosity of Gastric Mucus Glycoprotein in Cystic Fibrosis, *Digestion*, 1986, **34**(4), 275–280, DOI: **10.1159/000199341**.

35 S. Yang and G. A. Duncan, Synthetic Mucus Biomaterials for Antimicrobial Peptide Delivery, *J. Biomed. Mater. Res., Part A*, 2023, **111**(10), 1616–1626, DOI: **10.1002/jbm.a.37559**.

36 I. R. Dubbelboer, V. Barmpatsalou, A. Rodler, E. Karlsson, S. F. Nunes, J. Holmberg, J. Häggström and C. A. S. Bergström, Gastrointestinal Mucus in Dog: Physiological Characteristics, Composition, and Structural Properties, *Eur. J. Pharm. Biopharm.*, 2022, **173**, 92–102, DOI: **10.1016/j.ejpb.2022.02.019**.

586 | *J. Mater. Chem. B*, 2025, **13**, 577–587

This journal is © The Royal Society of Chemistry 2025

37 G. C. Hansson, Mucus and Mucins in Diseases of the Intestinal and Respiratory Tracts, *J. Intern. Med.*, 2019, **285**(5), 479–490, DOI: **10.1111/joim.12910**.

38 J. Koeevar-Nared, J. Kristl and J. Smid-Korbar, *Comparative Rheological Investigation of Crude Gastric Mucin and Natural Gastric Mucus*, 1997, vol. 18.

39 A. Luo, X. Liu, Q. Hu, M. Yang, H. Jiang and W. Liu, Efficacy of N-Acetylcysteine on Idiopathic or Postinfective Non-Cystic Fibrosis Bronchiectasis: A Systematic Review and Meta-Analysis Protocol, *BMJ Open*, 2022, **12**(3), e053625, DOI: **10.1136/bmjopen-2021-053625**.

40 F. Blasi, C. Page, G. M. Rossolini, L. Pallecchi, M. G. Matera, P. Rogliani and M. Cazzola, The Effect of *N*-Acetylcysteine on Biofilms: Implications for the Treatment of Respiratory Tract Infections, *Respir. Med.*, 2016, **117**, 190–197, DOI: **10.1016/j.rmed.2016.06.015**.

41 S. K. Lai, Y.-Y. Wang, D. Wirtz and J. Hanes, Micro- and Macrorheology of Mucus, *Adv. Drug Delivery Rev.*, 2009, **61**(2), 86–100, DOI: **10.1016/j.addr.2008.09.012**.

42 A. Darfeuille-Michaud, J. Boudeau, P. Bulois, C. Neut, A.-L. Glasser, N. Barnich, M.-A. Bringer, A. Swidsinski, L. Beaugerie and J.-F. Colombel, High Prevalence of Adherent-Invasive Escherichia Coli Associated with Ileal Mucosa in Crohn's Disease, *Gastroenterology*, 2004, **127**(2), 412–421, DOI: **10.1053/j.gastro.2004.04.061**.

43 D. Chokr, M. Cornu, C. Neut, C. Bortolus, R. Charlet, P. Desreumaux, S. Speca and B. Sendid, Adherent Invasive Escherichia Coli (AIEC) Strain LF82, but Not Candida Albicans, Plays a Profibrogenic Role in the Intestine, *Gut Pathog.*, 2021, **13**(1), 5, DOI: **10.1186/s13099-021-00401-z**.

44 V. Prudent, G. Demarre, E. Vazeille, M. Wery, N. Quenech'Du, A. Ravet, J. Dauverd-Girault, E. van Dijk, M.-A. Bringer, M. Descrimes, N. Barnich, S. Rimsky, A. Morillon and O. Espéli, The Crohn's Disease-Related Bacterial Strain LF82 Assembles Biofilm-like Communities to Protect Itself from Phagolysosomal Attack, *Commun. Biol.*, 2021, **4**(1), 627, DOI: **10.1038/s42003-021-02161-7**.

45 S. K. Shukla and T. S. Rao, An Improved Crystal Violet Assay for Biofilm Quantification in 96-Well Microtitre Plate, *bioRxiv*, 2017, preprint, DOI: **10.1101/100214**.

46 G. A. O'Toole, Microtiter Dish Biofilm Formation Assay, *J. Visualized Exp.*, 2011, **47**, 2437, DOI: **10.3791/2437**.

47 A. Sharma, N. Tyagi and R. Shrivastava, Optimization of Protocol for Quantification of Biofilm Formed by Pathogenic Rapidly-Growing Nontuberculous Mycobacteria for Diagnostic Screening, *Methods in Microbiology*, Academic Press Inc., 2023, vol. 53, pp. 67–99, DOI: **10.1016/bs.mim.2023.05.003**.

48 J. B. Kaplan, Biofilm Dispersal: Mechanisms, Clinical Implications, and Potential Therapeutic Uses, *J. Dent. Res.*, 2010, **89**(3), 205–218, DOI: **10.1177/0022034509359403**.

49 A. Zhao, J. Sun and Y. Liu, Understanding Bacterial Biofilms: From Definition to Treatment Strategies, *Front. Cell. Infect. Microbiol.*, 2023, **13**, DOI: **10.3389/fcimb.2023.1137947**.

50 K. P. Nickerson and C. McDonald, Crohn's Disease-Associated Adherent-Invasive Escherichia Coli Adhesion Is Enhanced by Exposure to the Ubiquitous Dietary Polysaccharide Maltodextrin, *PLoS One*, 2012, **7**(12), e52132, DOI: **10.1371/journal.pone.0052132**.

51 A. V. Nguyen, A. Y. Shourabi, M. Yaghoobi, S. Zhang, K. W. Simpson and A. Abbaspourrad, A High-Throughput Integrated Biofilm-on-a-Chip Platform for the Investigation of Combinary Physicochemical Responses to Chemical and Fluid Shear Stress, *PLoS One*, 2022, **17**, 1–17, DOI: **10.1371/journal.pone.0272294**.

This journal is © The Royal Society of Chemistry 2025

J. Mater. Chem. B, 2025, **13**, 577–587 | **587**